Ru(II) Complexes with Absorption in the PDT Window: $^1O_2$ Sensitization, DNA Binding, and Plasmid DNA Photocleavage

Sean J. Steinke, Marilyn N. Dunbar, M. Agustina Amalfi Suarez, Claudia Turro*

Department of Chemistry and Biochemistry, The Ohio State University, Columbus, Ohio 43210

Abstract. Two Ru(II) complexes, $[Ru(pydppn)(bim)(py)]^{2+}$ (**2**; pydppn = 3-(pyrid-2′-yl)-4,5,9,16-tetraaza-dibenzo[*a,c*]naphthacene; bim = 2,2'-bisimidazole; py = pyridine) and $Ru(pydppn)(Me_4bim)(py)]^{2+}$ (**3**; Me_4bim = 2,2'-bis(4,5-dimethylimidazole)), were synthesized and characterized, and their photophysical properties, DNA binding, and photocleavage were evaluated and compared to $[Ru(pydppn)(bpy)(py)]^{2+}$ (**1**; bpy = 2,2'-bipyridine). Complexes **2** and **3** exhibit broad ^{1}MLCT (metal-to-ligand charge transfer) transitions with maxima at ~470 nm and shoulders at ~525 nm and ~600 nm that extend to ~800 nm. These bands are red-shifted relative to those of **1**, attributed to the π-donating ability of the bim and Me_4bim ligands. A strong signal at 550 nm is observed in the transient absorption spectra of **1** – **3**, previously assigned as arising from a pydppn-centered $^3\pi\pi^*$ state, with lifetimes of ~19 μs for **1** and **2** and ~270 ns for **3**. A number of methods were used to characterize the mode of binding of **1** – **3** to DNA, including absorption titrations, thermal denaturation, relative viscosity changes, and circular dichroism, all of which point to the intercalation of the pydpppn ligand between the nucleobases. The photocleavage of plasmid pUC19 DNA was observed upon the irradiation of **1** – **3** with visible and red light, attributed to the sensitized generation of $^1O_2$ by the complexes. These findings indicate that the bim ligand, together with pydppn, serve to shift the absorption of Ru(II) complexes to the photodynamic therapy (PDT) window, 600 – 900 nm, and also extend the excited state lifetimes for the efficient production of cytotoxic singlet oxygen.

*Corresponding author: Claudia Turro, turro.1@osu.edu

Introduction

Photodynamic therapy (PDT) remains an important modality for cancer treatment that circumvents drawbacks of traditional chemotherapeutics, including systemic toxicity, drug resistance, and invasive procedures.[1] Ruthenium(II) complexes have played a prominent role in the development of PDT agents, including those that produce $^1O_2$ and other reactive oxygen species upon irradiation with visible light.[2–4] TLD1433 is a ruthenium(II) complex that has entered Phase II clinical trials for the treatment of bladder cancer when irradiated with green light.[5] Complexes of Ru(II) have also be designed to efficiently photodissociate a bioactive molecule, a modality commonly referred to as photochemotherapy (PCT).[6–9] In addition, complexes that are able to both produce $^1O_2$ and deliver a therapeutic agent are being developed.[10,11]

One area that remains a challenge for Ru(II) phototherapeutics is strong absorption in the red and near-IR spectral regions, the PDT window.[12–14] It was recently proposed that lowest-lying intra-ligand excited states are required to attain near-IR activity in Ru(II) complexes,[15] however, complexes that are operative from the lowest-energy triplet metal-to-ligand charge transfer (^{3}MLCT) excited state with $\lambda_{irr} \geq 650$ nm have been reported,[16] including one that undergoes one-photon ligand photodissociation with 735 nm irradiation,[17] and another with 760 nm.[18] The latter complexes possess a tridentate ligand with a central pyridine and two biquinoline substituents (dqpy) and an acetylacetonate (acac) or substituted acac ligand, and a photolabile nitrile, $[Ru(dqpy)(acac)(CH_3CN)]^{2+}$.[17] The π-donor acac ligand serves to raise the energy of the t_{2g}-type orbital set, also reducing the energy of the ^{3}MLCT state and affording near-IR absorption.[17]

In the present work, the coordination sphere around the Ru(II) center was designed to both sensitize the production of $^1O_2$ and shift the ^{1}MLCT absorption to longer wavelengths. In **2** and **3**, the tridentate ligand 3-(pyrid-2′-yl)-4,5,9,16-tetraaza-dibenzo[*a,c*]naphthacene (pydppn) was utilized, since it was previously shown to possess a long-lived $^3\pi\pi^*$ excited state below the ^{3}MLCT in Ru(II) complexes, resulting in the generation of $^1O_2$ and DNA photocleavage, attributed to both the production of the reactive species and strong DNA binding through intercalation.[19,20] In addition, the π-donor ligands 2,2'-bisimidazole (bim) and 2,2'-bis(4,5-dimethylimidazole) (Me_4bim) were used to reach the PDT window, with absorption beyond 600 nm. The complexes $[Ru(pydppn)(bim)(py)]^{2+}$ (**2**; py = pyridine) and $Ru(pydppn)(Me_4bim)(py)]^{2+}$ (**3**) were synthesized

and characterized, and their photophysical properties, DNA binding, and photocleavage were evaluated and compared to $[Ru(pydppn)(bpy)(py)]^{2+}$ (**1**; bpy = 2,2'-bipyridine)); the molecular structures of **1** – **3** are depicted in Figure 1.

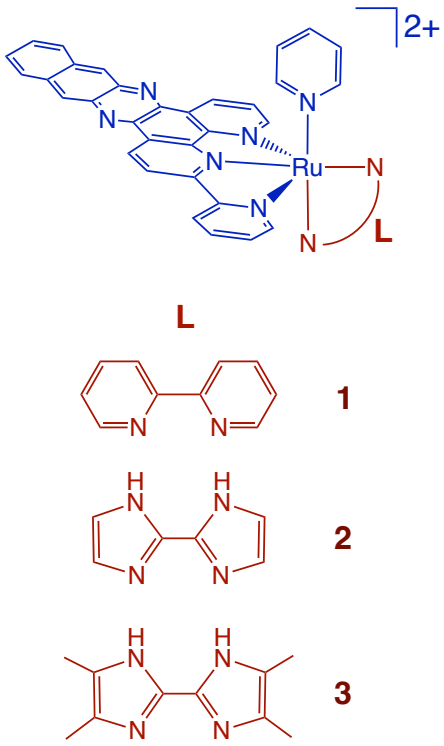

Figure 1. Schematic representations of the molecular structures of complexes **1** – **3**.

Experimental Section

Materials. All materials were used as received without further purification unless otherwise noted. Solvents were of reagent grade quality. Pyridine, dimethylformamide (DMF), diethyl ether, and methanol were purchased from Fisher Chemical. All deuterated solvents were purchased from Acros Organics. Lithium chloride, 2,2'-bisimidazole (bim), 2,2'-bis(4,5-dimethylimidazole) (Me-$_4$bim), 1,3-diphenylisobenzofuran (DPBF), calf-thymus DNA, sodium chloride, sodium phosphate, ethidium bromide, and Tris/HCl were purchased from Sigma Aldrich. Ammonium hexafluorophosphate was purchased from Oakwood Chemical, 200 proof ethanol was procured

from Decon Laboratories, and pUC19 plasmid was obtained from Bayou Biolabs and purified using the QIAprep Spin Miniprep Spin System from Qiagen. [Ru(pydppn)(bpy)(py)]$(PF_6)_2$,[21] pydppn,[19] $[Ru(tpy)_2]^{2+}$ (tpy = [2,2′;6′,2″]-terpyridine),[22] [Ru(pydppn)Cl_3],[21] and [Ru(p-cymene)(bim)Cl]Cl[23] were synthesized according to literature procedures.

[Ru(pydppn)(bim)(py)]$(PF_6)_2$ (2). [Ru(p-cymene)(bim)Cl]Cl (0.091 g, 0.20 mmol), pydppn (0.081 g, 0.20 mmol), and excess LiCl (0.095 g, 2.2 mmol) were combined in a minimal amount of DMF and heated to reflux under nitrogen in the dark for 2 hours. After cooling to room temperature, the reaction mixture was added dropwise to an aqueous solution of NH_4PF_6. The resulting solid was collected by vacuum filtration and washed with H_2O and Et_2O. The product was purified on a silica column and eluted with a 2:1 CH_2Cl_2/CH_3OH solvent mixture to afford [Ru(pydppn)(bim)Cl](PF_6) (0.021 g, 16%). [Ru(pydppn)(bim)Cl](PF_6) (0.021 g, 0.031 mmol) and excess pyridine (2 mL) in EtOH/H_2O (1:1, 20 mL) were heated to reflux under nitrogen in the dark overnight. After cooling to room temperature, EtOH was removed under reduced pressure, the remaining mixture was added dropwise to an aqueous solution of NH_4PF_6, and the resulting solid was collected by vacuum filtration. The product was washed with H_2O and Et_2O to yield [Ru(pydppn)(bim)(py)]$(PF_6)_2$ as a red-purple solid (0.013 g, 40%). ^{1}H NMR (400 MHz, CD_3OD, Figure S1): δ 9.44 (t, 2H, *J* = 8.7 Hz), 9.02 (d, 2H, *J* = 5.3 Hz), 8.98 (d, 1H, *J* = 8.4 Hz), 8.68 (d, 1H, *J* = 8.4 Hz), 8.31 (d, 1H, *J* = 5.1 Hz), 8.25 (m, 2H), 8.13 (dd, 3H, *J* = 10.9, 5.3 Hz), 8.05 (t, 1H, *J* = 7.5 Hz), 7.82 (dd, 1H, *J* = 5.3, 2.8 Hz), 7.68 (m, 6H), 7.54 (t, 1H, *J* = 6.5 Hz), 7.17 (t, 2H, *J* = 6.9 Hz), 7.04 (t, 1H, *J* = 6.6 Hz), 6.26 (s, 1H), 5.84 (s, 1H). ESI-MS(+): $[M - (PF_6)_2]^{2+}$ *m/z* = 362.097 (calc. *m/z* = 362.069).

[Ru(pydppn)(Me_4bim)(py)]$(PF_6)_2$ (3). [Ru(pydppn)Cl_3] (0.029 g, 0.047 mmol), Me_4bim (0.018 g, 0.096 mmol), and excess LiCl (0.070 g, 1.6 mmol) were combined in a EtOH/H_2O (3:1, 20 mL) mixture and heated to reflux under nitrogen in the dark for 4 hours. After cooling to room temperature, the solution was filtered to remove insoluble byproducts. EtOH was removed from the filtrate under reduced pressure and the crude product precipitated from H_2O by dropwise

addition of a concentrated aqueous NH_4PF_6 solution. The precipitate was collected via vacuum filtration and purified on a silica column. Elution with 6% CH_3OH/CH_2Cl_2 resulted in two purple bands which were collected and concentrated under reduced pressure. The residue was again purified on a neutral alumina column, eluted with 4% $MeOH/CH_2Cl_2$ and the leading purple band was collected. Solvent was removed under reduced pressure to afford [Ru(pydppn)(Me$_4$bim)Cl](PF$_6$) (0.014 g, 34%). [Ru(pydppn)(Me$_4$bim)Cl](PF$_6$) (0.014 g, 0.016 mmol) and excess pyridine (2 mL) in EtOH/H_2O (1:1, 20 mL) were heated to reflux under nitrogen in the dark overnight. After cooling to room temperature, EtOH was removed under reduced pressure and the desired product was precipitated by dropwise addition of a concentrated aqueous NH_4PF_6 solution. The resulting solid was collected by vacuum filtration and washed with H_2O and Et_2O to yield [Ru(pydppn)(Me$_4$bim)(py)](PF$_6$)$_2$ as a red-purple solid (0.013 g, 75%). ^{1}H NMR (400 MHz, CD_3OD, Figure S2): δ 9.45 (d, 1H, J = 7.8 Hz), 9.34 (d, 1H, J =8.4 Hz), 8.95 (m, 3H), 8.73 (d, 1H, J = 7.9 Hz), 8.46 (d, 1H, J = 5.5 Hz), 8.30 (d, 1H, J = 5.7 Hz), 8.24 (m, 2H), 8.17 (t, 1H, J = 7.7 Hz), 8.00 (d, 1H, J = 5.2 Hz), 7.93 (dd, 1H, J = 5.2, 3.2 Hz), 7.83 (d, 1H, J = 5.7 Hz), 7.66 (m, 4H), 7.09 (t, 2H, J = 6.9 Hz), 2.49 (m, 6H), 1.85 (s, 3H), 1.73 (s, 3H). ESI-MS(+): [M – PF$_6$)$_2$]$^{2+}$ m/z = 390.101 (calc. m/z = 390.100).

Instrumentation. ^{1}H NMR spectra were recorded using a Bruker DPX 400 MHz spectrometer and emission data were collected using a Horiba FluoroMax-4 fluorimeter. Electronic absorption spectra were obtained using an Agilent Cary 8454 or 8453 diode array spectrophotometer. Thermal denaturation studies used a Peltier temperature controlled sample cell and driver (HP89090A) controlled with Agilent UV-Vis ChemStation software. The home-built transient absorption instrument was previously reported and excitation was accomplished through the use of a frequency-doubled (532 nm) SpectraPhysics GCR-150 Nd:YAG laser (fwhm ~ 8 ns).[24] Relative viscosity measurements were performed using a Cannon-Manning semi-micro viscometer submerged in a water bath maintained at 25 °C by a Neslab model RGE-100 circulator. Circular dichroism spectra were obtained using a Jasco J-815 CD Spectrometer in 1x1 cm quartz cuvettes and electrospray ionization mass spectrometry (ESI-MS) was performed with a Bruker micrOTOF instrument with samples dissolved in acetonitrile and referenced to sodium trifluoroacetate. A 150

W Xe arc lamp in a (USHIO) in a MilliArc lamp housing unit, powered by a LPS-220 power supply and a LPS-221 igniter (PTI) was used for the DNA photocleavage experiments with $\lambda_{irr} \geq$ 395 nm. Photocleavage gels utilizing 655 nm were irradiated using 2 x 655 nm LEDs (Luceon Star Deep Red LEDs, LXM3-PD01, Lumiled) mounted on a SinkPAD-II 25 mm square base. Irradiation wavelengths for photocleavage experiments and emission wavelengths for $^1O_2$ quantum yield measurements were controlled with long-pass filters (CVI Melles Griot). The ethidium bromide-stained agarose gels were imaged using a Gel Doc 2000 transilluminator (BioRad) operated with Quantity One (v. 4.1.1) software and a GelDoc Go Imaging System (BioRad).

Methods. All photophysical measurements were performed in 1× 1 cm quartz cuvettes. Singlet oxygen quantum yields were performed using $[Ru(bpy)_3]^{2+}$ as a standard (Φ_Δ = 0.81 in MeOH), 1,3-diphenylisobenzofuran (DPBF) as a $^1O_2$ trapping agent, and following a previously detailed procedure.[25] Samples for transient absorption measurements were prepared with an absorbance of 0.2 – 0.4 at 532 nm, the excitation wavelength, in Kontes top quartz cuvettes and sparged for 15 min with N_2 prior to each measurement. Relative viscosity and electronic absorption titrations were performed using calf-thymus DNA (CT-DNA) purified overnight by dialysis against 5 mM Tris buffer (50 mM NaCl, pH 7.0), while DNA melting temperature, T_m, measurements were performed using CT-DNA purified overnight by dialysis against 1 mM PO_4 buffer (1 mM NaCl, pH 7.4). DNA binding constants, K_b, of complexes **1** – **3** were determined by room temperature spectrophotometric titration of 20 μM of **1** or 12 μM of **2** or **3** CT-DNA with 0 to 250 μM CT-DNA (5 mM Tris, 50 mM NaCl, pH 7.0). The value of K_b was calculated by fitting the resulting data to eq 1

$$\frac{\varepsilon_a-\varepsilon_f}{\varepsilon_b-\varepsilon_f} = \frac{b-\left(b^2-2K_b^2C_t[DNA]_t/s\right)^{1/2}}{2K_bC_t} \quad (1)$$

where $b = 1 + K_bC_t + K_b[\text{DNA}]_t/2s$, C_t is the total complex concentration, $[\text{DNA}]_t$ is the total CT-DNA concentration, s is the base pair binding site size, and ε_a, ε_b, and ε_f are the apparent, free, and bound complex molar extinction coefficients, respectively.[26] The value of ε_b was determined from the point at which addition of CT-DNA did not result in further changes in the absorption spectrum.

Relative viscosity measurements were performed using sonicated CT-DNA that was an average length of ~200 base pairs in order to minimize DNA flexibility.[27] For these experiments,

the ratio of metal complex or ethidium bromide concentration to DNA was increased by adding small volumes of concentrated stock solutions to the sample already in the viscometer. Solutions in the viscometer were mixed by bubbling with nitrogen and were allowed to equilibrate to 25 °C in the water bath for 30 minutes prior to each measurement. The relative viscosities, η, at a given [Complex]:[DNA] ratio or that for measured for DNA alone, η_0, were calculated from eq 2,

$$\eta = \frac{(t - t_0)}{t_0} \quad (2)$$

where *t* is the flow time of a given solution containing DNA and t_0 is the flow time of buffer alone. Relative viscosity data are plotted as $(\eta/\eta_0)^{1/3}$ as a function of the ratio of complex to DNA concentration, [Complex]:[DNA].[28]

Thermal denaturation experiments were performed using 100 μM CT-DNA and 2 μM Ru(II) complex (1 mM phosphate, 1 mM NaCl, pH 7.4). The absorbance at 260 nm was monitored as a function of temperature, which was increased in 1 °C increments from 40 to 80 °C and was held for 1 minute at each step prior to each measurement. The instrument software determined the melting temperature by fitting absorbance data to a sigmoidal function; the T_m values are reported as the average of the inflection point of the sigmoidal curve of three separate trials.

For circular dichroism (CD) experiments, each Ru(II) complex was titrated into a 100 μM CT-DNA solution (1 mM phosphate, 1 mM NaCl, pH 7.4), followed by thorough mixing and allowing the solution to equilibrate for 10 min prior to recording the spectra under ambient conditions. High frequency noise was filtered out using Jasco SpectraAnalysis software and all spectra were collected in triplicate.

DNA photocleavage experiments were performed using 20 μL total solution volume in transparent 500 μL Eppendorf tubes containing 100 μM pUC18 or pUC19 plasmid and the specified concentration of Ru(II) complex (5 mM Tris buffer, 50 mM NaCl, pH 7.4). Irradiation of the samples was performed under ambient conditions, followed by the addition of 4 μL DNA gel loading buffer to each sample. Samples were loaded onto 1% w/v agarose gels stained with 0.5 mg/L ethidium bromide and electrophoresis was performed in 1× TAE buffer (40 mM Tris-acetate, 1 mM EDTA, pH ~8.2).

Results and Discussion

Photophysical Properties

Complexes **2** and **3** exhibit strong absorption throughout the visible region, similar to **1**, as shown in Figure 2. Each complex exhibits a strong pydppn-centered $^1\pi\pi^*$ transition at ~410 nm (Figure 2), as previously reported for **1**.[21] Broad Ru(dπ) → pydppn(π*) ^{1}MLCT transitions centered at 452 nm (ε = 10,150 M^{-1} cm^{-1}) and 480 nm (ε = 10,200 M^{-1} cm^{-1}) are observed in **1**, which shift to 471 nm (ε = 8,700 M^{-1} cm^{-1}) and ~520 nm (sh; ε ~ 6,000) in **2**, and to 464 nm (6,500 M^{-1} cm^{-1}) and ~520 nm (sh; ε ~ 5,000) in **3** (Figure 2). The red shift of the higher energy band from **1** to **2** of ~900 cm^{-1} is similar to that reported for the ^{1}MLCT transitions in related complexes and attributed to the greater π-donating ability of bim as compared to bpy.[29,30] For example, a shift in the Ru(dπ) → tpy(π*) band from 468 nm to 491 nm was observed between $[Ru(tpy)(bpy)(py)]^{2+}$ and $[Ru(tpy)(bim)(py)]^{2+}$ in acetone (Δ ~ 1,000 cm^{-1}),[31] as well as for the Ru(dπ) → bpy(π*) ^{1}MLCT transitions in $[Ru(bpy)_3]^{2+}$ and $[Ru(bpy)_2(bim)]^{2+}$ in CH_3CN, from 452 nm to 473 nm, respectively, Δ ~ 980 cm^{-1}.[32] It should be noted that the Ru(dπ) → bim(π*) absorption is expected at higher energies based on the 396 nm (ε = 10,700 $M^{-1}cm^{-1}$) maximum reported for $[Ru(bim)_3]^{2+}$ in H_2O and that at 340 nm (ε = 10,700 $M^{-1}cm^{-1}$) reported for $[Ru(bpy)_2(bim)]^{2+}$ in CH_3CN.[32,33] A red shift is also observed in the Ru(dπ) → pydppn(π*) ^{1}MLCT absorption maximum of **3** relative to that of **1**, as previously reported for the related tpy complexes. [23,31] In addition, absorption bands are observed at 620 nm (2,100 M^{-1} cm^{-1}) in **2** and at 583 nm (2,600 $M^{-1}cm^{-1}$), that are also present in the spectra of $[Ru(tpy)(bim)(py)]^{2+}$ and of $[Ru(tpy)(Me_4bim)(py)]^{2+}$,[31] such that they may be assigned as arising from ^{1}MLCT transitions to the tridentate ligand (Figure 2). As a result, complexes **2** and **3** have absorptions that tail to ~800 nm, reaching into the PDT window.

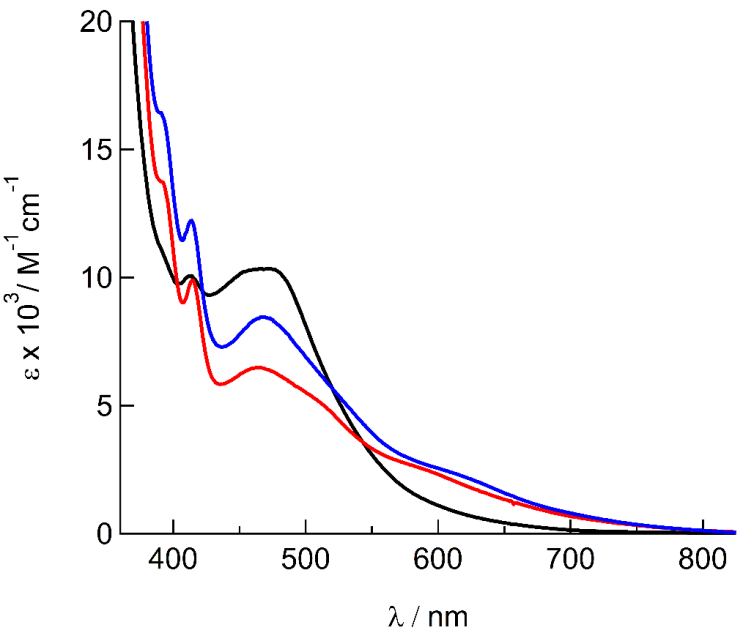

Figure 2. Electronic absorption spectra of **1** (black), **2** (blue), and **3** (red) in acetone.

Complexes **1** – **3** are not emissive at room temperature, such that their excited state dynamics were investigated using nanosecond transient absorption (TA) spectroscopy in deaerated CH_3CN. The TA spectra of **1** and **2** are shown in Figure 3, both of which exhibit a strong excited state absorption at 550 nm. The signal at 550 nm observed for each complex was fitted to a monoexponential decay monoexponentially resulting in lifetimes, τ of 19 μs and 18 μs for **1** and **2**, respectively. These features and lifetimes are consistent with a pydppn-centered $^3\pi\pi^*$ excited state, observed previously in $[Ru(tpy)(pydppn)]^{2+}$ (τ = 18 μs, CH_3CN) and $[Ru(pydppn)_2]^{2+}$ (τ = 23 μs, CH_3CN).[19] The long-lived $^3\pi\pi^*$ excited states of **1** and **2** produce cytotoxic $^1O_2$ following irradiation with 460 nm under ambient conditions, with quantum yields, Φ_Δ, of 0.53(2) and 0.44(2), respectively.

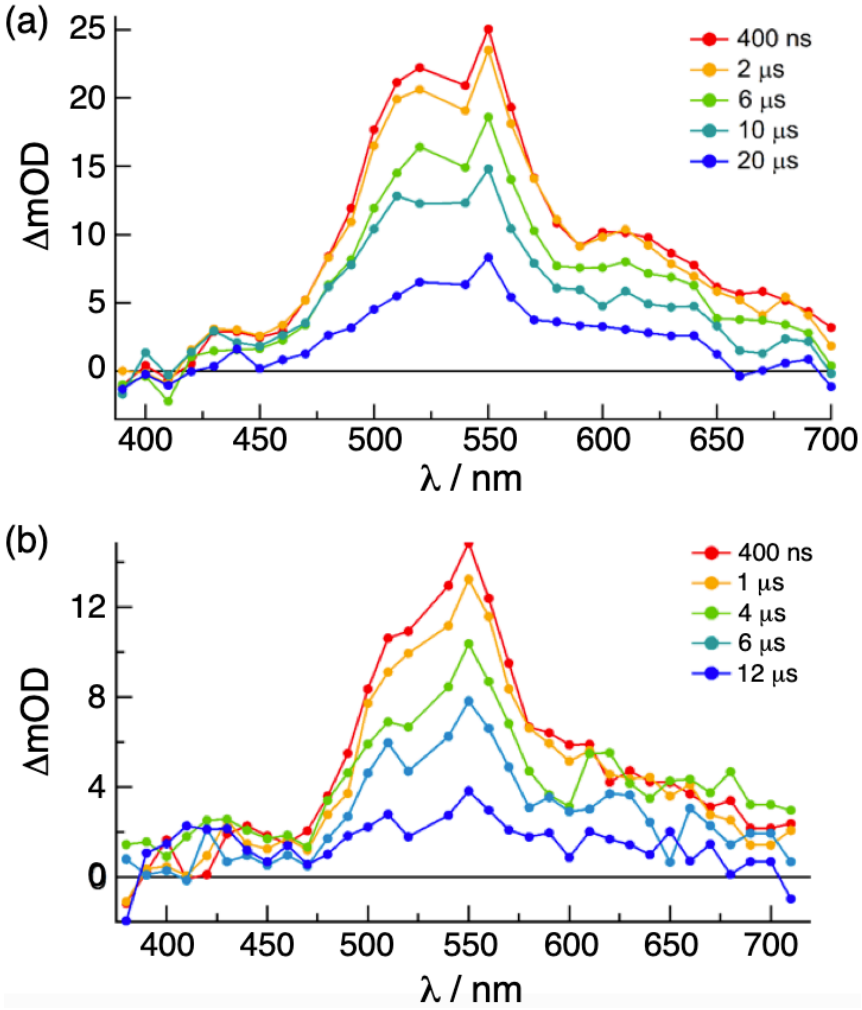

Figure 3. Transient absorption spectra of (a) **1** and (b) **2** in deaerated CH_3CN (λ_{ex} = 532 nm, 4 mJ/pulse, fwhm = 8 ns).

Unlike the long lifetimes observed with **1** and **2**, τ = 267 ns was measured for **3** in deaerated CH_3CN,which also exhibits the characteristic TA feature associated with the pydppn $^3\pi\pi^*$ state centered at 550 nm (Figure 4a). The short lifetime for **3** can be explained by the decomposition of the complex upon irradiation (Figure 4b), indicating that the presence of the Me_4bim ligand in **3** causes photodecomposition reactions under an anerobic environment. Attempts to determine Φ_Δ for **3** were unsuccessful, since the signal from the complex rapidly decreased in intensity during the experiment. However, given the observed changes in the emission signal of DPBF it is clear that **3** produces $^1O_2$ upon irradiation. Li et al. previously found that low energy irradiation of *cis*–$[Ru(bpy)_2(Me_4bim)]^{2+}$ in the presence of oxygen led to the rapid decomposition of the Me_4bim

ligand through a [4 + 2] cycloaddition of $^1O_2$.[34] It was concluded that **3** undergoes a similar process of decomposition when irradiated in the presence of O_2, in addition to different photodecomposition processes that must also be operative in **3** when deaerated, as evidenced by the decomposition shown in Figure 4b.

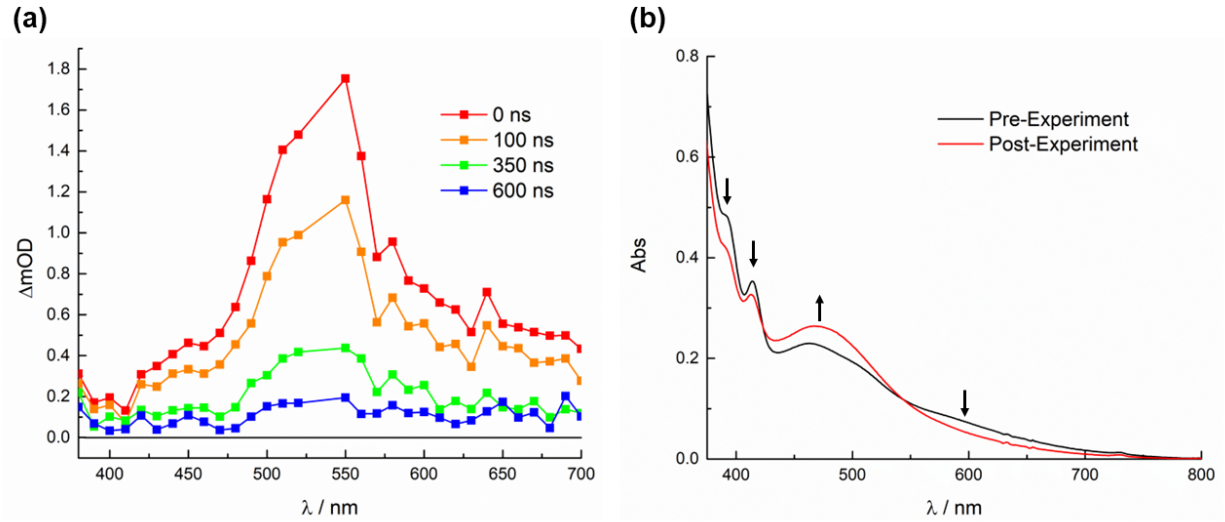

Figure 4. (a) Transient absorption spectra of **3** in deaerated CH_3CN (λ_{ex} = 532 nm, 1 mJ/pulse, fwhm = 8ns) and (b) electronic absorption spectra of **3** before and after the transient absorption experiment.

It should be noted that although the lowest energy ^{1}MLCT Ru(dπ) → pydppn(π*) transition in **2** and **3** at 583 nm is observed at a significantly lower energy than the 410 nm ^{1}ππ* pydppn absorption, the TA spectrum of **2** and **3** is clearly that of the ^{3}ππ* state of pydppn. In $[Ru(bpy)_3]^{2+}$, the ^{3}MLCT state lies ~5,000 cm^{-1} below the corresponding ^{1}MLCT. Assuming a similar energy difference between the singlet and triplet Ru → pydppn MLCT states in **2** and **3**, the ^{3}MLCT state may be estimated to lie ~12,500 cm^{-1} (~1.55 eV) above the ground state, ^{1}GS. In prior work from the Turro group, the energy of the ^{3}ππ* state of pydppn was estimated to be ~1.5 eV from energy transfer quenching experiments,[19] such that this state must lie just below the Ru → pydppn ^{3}MLCT in **2** and **3**.

DNA Binding and Photocleavage

Cationic ruthenium complexes have been shown to interact with DNA in a number of ways, including noncovalent Coulombic or electrostatic attraction and intercalation,[35,36] however, it has been establish that a number of methods must be taken together to ascertain the DNA binding mode.[37] The changes in the electronic absorption spectra of 20 μM of **2** and 12 μM of **1** and **3** upon the addition of up to 200 μM bases of CT-DNA were used to calculate the DNA binding constant, K_b, of each complex using eq 1 (Figure S4). The fits resulted in K_b = 7.5(9) x 10^5 M^{-1} (s = 1.4 ± 0.2) for **1**, 1.8(8) x 10^6 M^{-1} (s = 1.5 ± 0.8) for **2**, and 2.6(9) x 10^5 M^{-1} (s = 0.35 ± 0.07) for **3**. These values are similar to those reported for intercalating Ru(II) polypyridyl complexes containing ligands with extended π-systems, with K_b values of 3.5 × 10^5 M^{-1} for $[Ru(pydppn)_2]^{2+}$,[19] 2 × 10^6 M^{-1} for $[Ru(tpy)(pydppz)]^{2+}$,[20] and 1 – 5 × 10^6 M–1 for *cis*–$[Ru(phen)_2(dppz)]^{2+}$ (phen = 1,10-phenanthroline),[26,38] as well as divalent Ru(II) complexes containing dppz and its derivatives,[39,40] and those possessing dppn and substituted dppn ligands with K_b = 5.7 – 8.0 × 10^5 M^{-1}.[41] Therefore, the hypochromic and bathochromic shifts observed in the absorption spectra of **1** – **3** upon addition of CT-DNA and the resulting binding constants are consistent with complexes that intercalate between the DNA bases (Figures S3 – S5), however, π-stacking of cationic complexes on the DNA surface aided by the presence of the polyanionic backbone has been previously reported.[43] Therefore, additional methods must be utilized to unequivocally show intercalation of **1** –**3**.

Thermal denaturation experiments provide an indication of the strength of hydrogen bonding and π-stacking interactions that stabilize double-stranded DNA (ds-DNA), such that as the solution is heated, there is a point in which the double helix "melts" into its single-strand components, ss-DNA, known as the DNA melting temperature, T_m. The presence of complexes that interact with DNA only through electrostatic interactions typically do not significantly affect the value of T_m, whereas the enhanced π-interactions that take place when a molecule intercalates requires higher temperatures for the two strands to dissociate.[42,43] The changes to the DNA absorption at 260 nm provide a measure of the conversion of ds-DNA to ss-DNA, since the breaking of the duplex π-stacking results in greater absorption by the nucleobases. Thermal denaturation experiments of 100 μM CT-DNA alone in solution and in the presence of 2 μM **1** – **3** are shown in Figure 5 (1 mM phosphate, 1 mM NaCl, pH 7.4). In the absence of Ru(II) complex, T_m = 60.4(6) °C was recorded , whereas higher T_m values were measured in the presence of each complex, **1** – **3**, 65(2) °C, 65(1) °C, and 66(1) °C, respectively. Shifts in the melting temperature,

ΔT_m values of 5–6 °C were previously reported for divalent DNA intercalators,[26,44–46] however, these values are highly dependent on ionic strength and [DNA]:[probe] ratio, such that greater DNA stabilization has been published for many complexes of dppz, dppn, and their derivatives.[43,47,48]

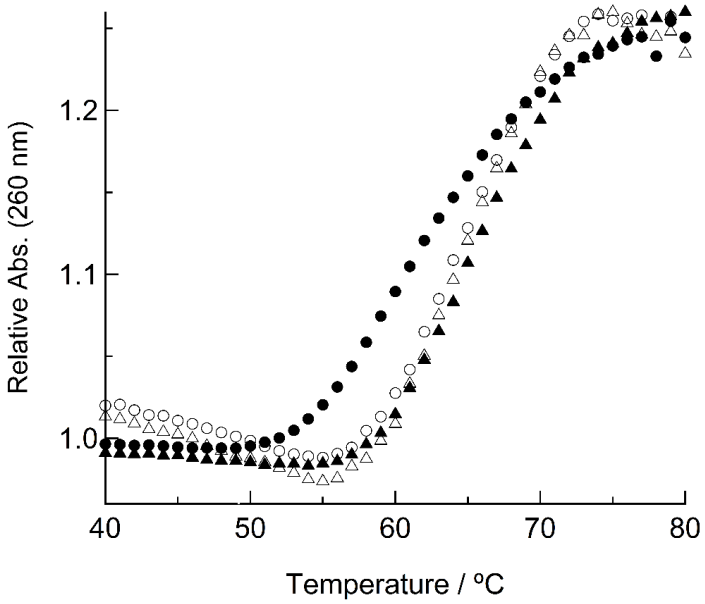

Figure 5. Thermal denaturation of 100 μM CT-DNA alone (●) and in the presence of 2 μM **1** (Δ), **2** (○), and **3** (▲) in 1 mM phosphate buffer (1 mM NaCl, pH 7.4).

Relative viscosity experiments were performed on DNA solutions in the presence of **1** – **3** and the results were compared to those for the intercalator ethidium bromide (EtBr) and the $[Ru(tpy)_2]^{2+}$, which binds to DNA through electrostatic interactions. As expected for an intercalator that unwinds and lengthens the double helix, [37,49] an increase in the relative viscosity is evident from Figure 6 with the concentration of EtBr, whereas no changes are observed under similar experimental conditions for $[Ru(tpy)_2]^{2+}$. The addition of **1** – **3** to solutions of DNA results in an increase of the relative viscosity, indicative of intercalation, as previously reported for related complexes.[43,50–52]

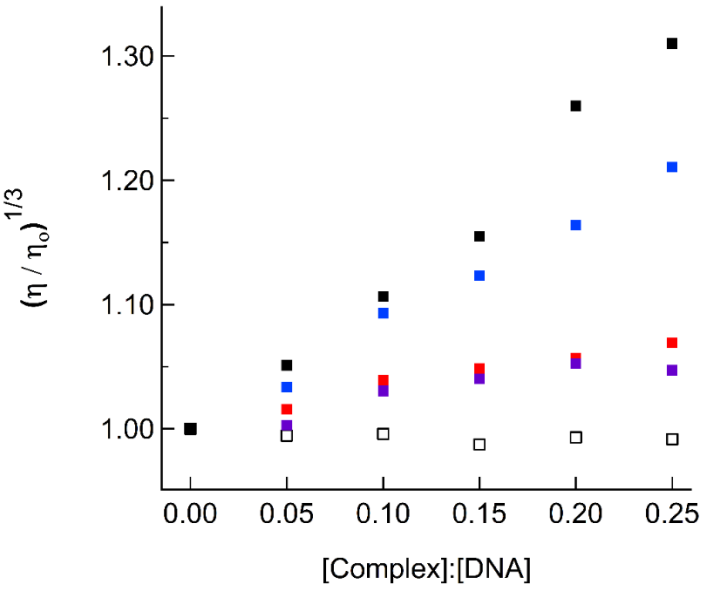

Figure 6. Changes in the relative viscosity of solutions containing 200 μM CT-DNA as a function of increasing concentration of ethidium bromide (solid black), $[Ru(tpy)_2]^{2+}$ (black, open), **1** (filled, blue), **2** (filled, red), and **3** (filled, purple).

Circular dichroism (CD) experiments were performed to further characterize the interactions between **1** – **3** with CT-DNA. The interaction of CT-DNA with circularly polarized light results in characteristic CD signals, a negative feature at 245 nm associated with the helical B-DNA structure and a positive absorption at 275 nm related to base stacking, as shown in Figure 6 for 100 μM CT-DNA in 1 mM phosphate buffer (blue trace; pH 7.4).[53,54] Achiral molecules, such as **1** – **3**, do not interact with polarized light themselves, but their interactions with chiral DNA can result in induced circular dichroism (ICD) at wavelengths where the probe absorbs, as previously shown for EtBr upon DNA intercalation.[55,56] The CD spectrum of 50 μM **2** and 100 μM CT-DNA in 1 mM phosphate (pH = 7.4) with 1 mM NaCl is shown in Figure 7a (dashed, red trace), where strong ICD features are observed at 335 nm and 370 nm associated with pydppn-centered $^1\pi\pi^*$ transitions, along with a smaller band centered at ~295 nm previously reported with intercalating dppz ligands.[54,57]

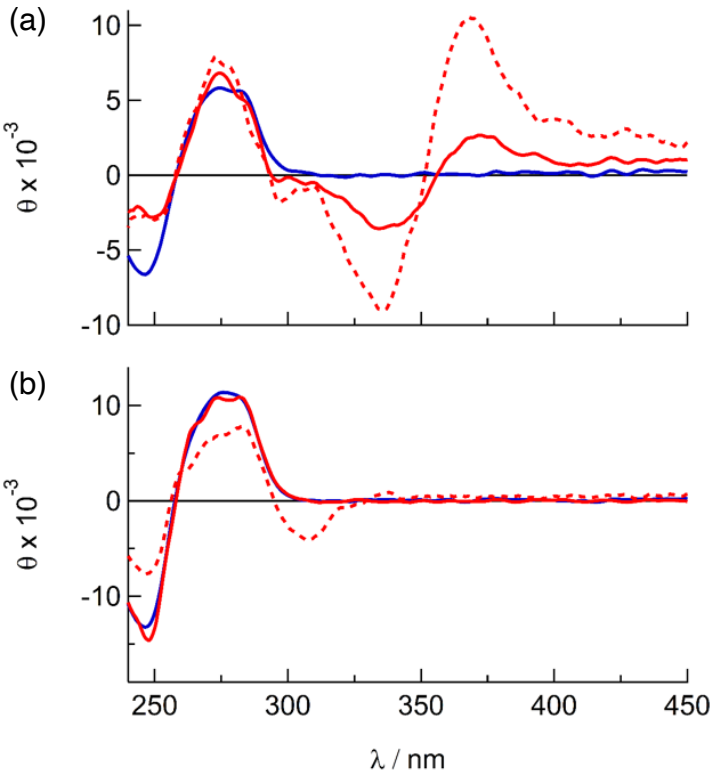

Figure 7. CD Spectra of 100 μM CT-DNA (alone (blue), and in the presence of (a) 50 μM **2** and (b) 50 mM $[Ru(tpy)_2]^{2+}$ with 1 mM NaCl (dashed, red) and 50 mM NaCl (solid, red) in 1 mM phosphate buffer (pH 7.4).

To ensure that electrostatic interactions were not playing a role in the observed ICD signals, $[Ru(tpy)_2]^{2+}$ was used as a control, which does not intercalate between the DNA bases.[20,58] In the presence of 50 μM $[Ru(tpy)_2]^{2+}$ and 1 mM NaCl, the CD spectrum of 100 μM CT-DNA in 1 mM phosphate buffer (pH = 7.4) shown in Figure 7b (dashed, red trace) exhibits an ICD band at 310 nm associated with a tpy-centered $^1\pi\pi^*$ transition. However, when the ionic strength is increased using 50 mM NaCl, the ICD feature disappears and only the CD spectrum typical of CT-DNA is observed (Figure 7b; solid, red trace). It is evident from the CD spectrum recorded for 50 μM **2** and 100 μM CT-DNA in the presence of 50 mM NaCl shown in Figure 7a (solid, red trace), that the $^1\pi\pi^*$ pydppn ICD features are weaker as compared to those at lower ionic strength, but are clearly observed. Similar results are observed for **1** and **3** (Figures S6 and S7). These data, together with the absorption titrations, relative viscosity changes, and the thermal denaturation results, are

consistent with electrostatic interactions between $[Ru(tpy)_2]^{2+}$ and CT-DNA, but with pydppn intercalation by **1** – **3**.

Agarose gel electrophoresis was used to assess the ability of **1** – **3** to photocleave plasmid DNA upon visible light irradiation ($\lambda_{irr} \geq 395$ nm) and low-energy irradiation ($\lambda_{irr} = 655$ nm) in 5 mM Tris buffer (50 mM NaCl, pH 7.4).

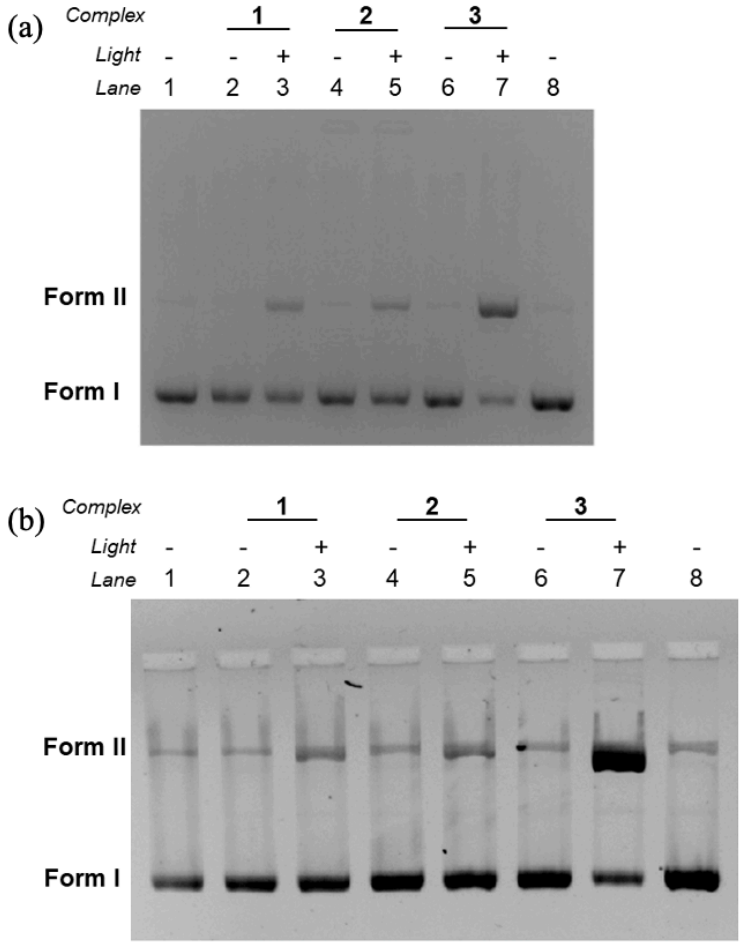

Figure 8. Ethidium bromide stained agarose gel (1% w/v) of 100 μM bases in (a) pUC19 and (b) pUC18 alone (lanes 1 and 8) and in the presence of 5 μM **1** (lanes 2 and 3), **2** (lanes 4 and 5), and **3** (lanes 6 and 7), kept in the dark (lanes 2, 4, and 5) or irradiated (lanes 3, 5, and 7) with (a) t_{irr} = 25 min, $\lambda_{irr} \geq 395$ nm, (b) t_{irr} = 25 min, $\lambda_{irr} = 655$ nm (5 mM Tris, 50 mM NaCl, pH 7.4).

Lanes 1 and 8 of Figure 8 contain undamaged supercoiled pUC18 or pUC19 plasmid (100 μM bases, Form I) in the absence of metal complex, which also contain a small amount of single-strand, nicked impurity (Form II). In the presence of 5 μM **1**, **2**, and **3** in the dark, lanes 2, 4, and

6, respectively, no additional cleavage product is observed (Figure 8). In contrast, it is evident in Figure 8 that the irradiation of 5 μM **1** – **3** in containing 100 μM pUC19 (lanes 3, 5, and 7, respectively) for 25 min with both visible and red light results in an increase in the amount of nicked, open circular DNA (Form II). The observed DNA photocleavage can be attributed to the production of cytotoxic $^1O_2$, as previously reported for related complexes.[25,59,60] The band associated with form II plasmid DNA in lane 7 is darker than the corresponding bands in lanes 3 and 5, indicating that complex **3** may cleave plasmid DNA to a greater extent than **1** or **2**. This difference could be due to a higher efficiency of $^1O_2$ production or the generation of a reactive decomposition product that is currently unknown.

Conclusions

Two Ru(II) complexes, $[Ru(pydppn)(bim)(py)]^{2+}$ (**2**; pydppn = 3-(pyrid-2′-yl)-4,5,9,16-tetraaza-dibenzo[*a,c*]naphthacene; bim = 2,2'-bisimidazole; py = pyridine) and $Ru(pydppn)(Me_4bim)(py)]^{2+}$ (**3**; Me_4bim = 2,2'-bis(4,5-dimethylimidazole), were synthesized and characterized. The photophysical properties, DNA binding, and photocleavage of **2** and **3** were evaluated and compared to those of $[Ru(pydppn)(bpy)(py)]^{2+}$ (**1**; bpy = 2,2'-bipyridine). Complexes **2** and **3** exhibit broad ^{1}MLCT (metal-to-ligand charge transfer) with maxima at ~470 nm and shoulders at ~525 nm and ~600 nm that extend to ~800 nm. These bands are red-shifted relative to those of **1**. The shift in the ^{1}MLCT absorption to lower energies is attributed to the π-donating ability of the bim and Me_4bim ligands. A strong signal at 550 nm is observed in the transient absorption spectra of **1** and **2**, previously assigned as arising from a pydppn-centered $^3\pi\pi^*$ state, with lifetimes of ~19 μs. The transient absorption spectrum of **3** showed a similar signal at 550 nm but the lifetime was ~270 ns, which likely arises from rapid sample decomposition upon irradiation, however, it was determined that **1** – **3** generate $^1O_2$ upon irradiation with visible and red light. A number of methods were used to characterize the DNA binding mode of **1** – **3**, including absorption titrations, thermal denaturation, relative viscosity changes, and circular dichroism, all of which point to the intercalation of the pydpppn ligand between the nucleobases. The absorption titration were used to obtatin DNA binding constants, resulting in K_b = 7.5(9) x 10^5 M^{-1} (s = 1.4 ± 0.2) for **1**, 1.8(8) x 10^6 M^{-1} (s = 1.5 ± 0.8) for **2**, and 2.6(9) x 10^5 M^{-1} (s = 0.35

± 0.07) for **3**. The photocleavage of plasmid DNA was observed upon the irradiation of **1** – **3** with visible and red light, attributed to the sensitized generation of $^1O_2$ by the complexes. These findings indicate that the bim ligand, together with pydppn, serve to shift the absorption of Ru(II) complexes to the photodynamic therapy (PDT) window, 600 – 900 nm, and also extend the excited state lifetimes for the efficient production of cytotoxic singlet oxygen.

Acknowledgments. We gratefully acknowledge the partial support of the National Science Foundation (CHE 2102508).

Supporting Information. The Supporting Information is available free of charge on the internet. ^{1}H NMR spectral data; DNA binding titrations; additional CD spectra.

References

(1) Kaur, R.; Bhardwaj, A; Gupta, S. Cancer Treatment Therapies: Traditional to Modern Approaches to Combat Cancers. *Mol. Biol. Reports* **2023**, *50*, 9663–9675.

(2) Conti, L.; Macedi, E.; Giorgi, C.; Valtancoli, B.; Fusi, V. Combination of Light and Ru(II) Polypyridyl Complexes: Recent Advances in the Development of New Anticancer Drugs. *Coord. Chem. Rev.* **2022**, *469*, 214656.

(3) Grandioso, A.; Purkait, K.; Gasser, G. Recent Approaches Towards the Development of Ru(II) Polypyridyl Complexes for Anticancer Photodynamic Therapy. *Chimia* **2021**, *75*, 845–855.

(4) Cole, H. D.; Vali, A.; Roque III, J. A.; Shi, Ge; Kaur, G.; Hodges, R. O.; Francés-Monerris, A.; Alberto, M. E.; Cameron, C. G.; McFarland, S. A. Ru(II) Phenanthroline-Based Oligothienyl Complexes as Phototherapy Agents. *Inorg. Chem.* **2023**, *62*, 21181–21200.

(5) Monro, S.; Colón, K. L.; Yin, H.; Roque III, J.; Konda, P.; Gujar, S.; Thummel, R. P.; Lilge, L.; Cameron, C. G.; McFarland, S. A. Transition Metal Complexes and Photodynamic Therapy from a Tumor-Centered Approach: Challenges, Opportunities, and Highlights from the Development of TLD1433. *Chem. Rev.* **2019**, *119*, 797–828.

(6) (a) Bonnet, S. Ruthenium-Based Photoactivated Chemotherapy. *J. Am. Chem. Soc.* **2023**, *145*, 23397–23415. (b) Hakkennes, M. L. A.; Meijer, M. S.; Menzel, J. P.; Goetz, A.-C.; Van Duijn, R.; Siegler, M. A.; Buda, F.; Bonnet, S. Ligand Rigidity Steers the Selectivity and Efficiency of the Photosubstitution Reaction Strained Ruthenium Polypyridyl Complexes. *J. Am. Chem. Soc.* **2023**, *145*, 13420–13434.

(7) Knoll, J. D.; Turro, C. Control and Utilization of Ruthenium and Rhodium Metal Complex Excited States for Photoactivated Cancer Therapy. *Coord. Chem. Rev.* **2015**, *282-283*, 110–126.

(8) (a) Toupin, N.; Steinke, S. J.; Nadella, S.; Li, A.; Rohrabaugh Jr., T. N.; Samuels, E. R.; Turro, C.; Sevrioukova, I. F.; Kodanko, S. J. Photosensitive Ru(II) Complexes as Inhibitors of the Major Human Drug Metabolizing Enzyme CYP3A4. *J. Am. Chem. Soc.* **2021**, *143*, 9191–9205. (b) Li, A.; Turro, C.; Kodanko, J. J. Ru(II) Polypyridyl Complexes Derived from Tetradentate Ancillary Ligands for Effective Photocaging. *Acc. Chem. Res.* **2018**, *51*, 1415–1421. (c) Respondek, T.; Garner, R. N.; Herroon, M. K.; Podgorski, I.; Turro, C.; Kodanko, J. J. Light Activation of a Cysteine Protease Inhibitor: Caging of a Peptomimetic Nitrile with $Ru^{II}(bpy)_2$. *J. Am. Chem. Soc.* **2011**, *133*, 17164–17167.

(9) Garner, R. N.; Galllucci, J. C.; Dunbar, K. R.; Turro, C. $[Ru(bpy)_2(5\text{-cyanouracil})_2]^{2+}$ as a Potential Light-Activated Dual-Action Theraputic Agent. *Inorg. Chem.* **2011**, *50*, 9213–9215.

(10) (a) Steinke, S. J.; Kodanko, J. J.; Turro, C. Ruthenium Complexes for Photoactivated Dual Activity: Drug Delivery and Singlet Oxygen Generation. *Adv. Inorg. Chem.* **2022**, *80*, 285–320. (b) Arora, K.; Herroon, M.; Al-Afyouni, M. H.; Toupin, N. P.; Rohrabaugh Jr., T. N.; Loftus, L. M.; Podgorski, I.; Turro, C.; Kodanko, J. J. Catch and Release Photosensitizers: Combining Dual-Action Ruthenium Complexes with Protease Inactivation for Targeting

Invasive Cancers. *J. Am. Chem. Soc.* **2018**, *140*, 14367–14380. (c) Knoll, J. D.; Albani, B. A.; Turro, C. Excited State Investigation of a New Ru(II) Complex for Dual Reactivity with Low Energy Light. *Chem. Commun.* **2015**, *51*, 8777–8780.

(11) (a) Albani, B. A.; Peña, B.; Leed, N. A.; de Paula, N. A. B. G.; Pavani, C.; Baptista, M. S.; Dunbar, K. R.; Turro, C. Marked Improvement in Photoinduced Cell Death by a New Tris-heteroleptic Complex with Dual Action: Singlet Oxygen Sensitization and Ligand Dissociation. *J. Am. Chem. Soc.* **2014**, *136*, 17095–17101. (b) Sgambellone, M. A.; David, A.; Garner, R. N.; Dunbar, K. R.; Turro, C. Cellular Toxicity Induced by the Photorelease of a Caged Bioactive Molecule: Design of a Potential Dual-Action Ru(II) Complex. *J. Am. Chem. Soc.* **2013**, *135*, 11274–11282.

(12) Banerjee, S. Polypyridyl Ruthenium(II) Complexes with Red-Shifted Absorption: New Promises in Photodynamic Therapy. *ChemBioChem* **2021**, *22*, 2407–2409.

(13) Heinemann, F.; Karges, J.; Gasser, G. Critical Overview of the Use of Ru(II) Polypyridyl Complexes as Photosensitizers in One-Photon and Two-Photon Photodynamic Therapy. *Acc. Chem. Res.* **2017**, *50*, 2727–2736.

(14) Kessel, D. Critical PDT Theory VII: The Saga of Ruthenium. *Photodiag. Photodyn. Ther.* **2023**, *42*, 103615.

(15) Lifshits, L. M.; Roque III, J. A.; Ramasamy, E.; Thummel, R. P.; Cameron, C. G.; McFarland, S. A. Ruthenium Photosensitizers for NIR PDT Require Lowest-Lying Triplet Intraligand (^{3}IL) Excited States. *J. Photochem. Photobiol.* **2021**, *8*, 100067.

(16) Loftus, L. M.; Al-Afyouni, K. F.; Turro, C. New Ru^{II} Scaffold for Photoinduced Ligand Release with Red Light in the Photodynamic Therapy (PDT) Window. *Chem. Eur. J.* **2018**, *24*, 11550–11553.

(17) Al-Ayouni, M. H.; Rohrabugh Jr., T. N.; Al-Afyouni, K. F.; Turro, C. New Ru(II) Photocages Operative with Near-IR Light: New Platform for Drug Delivery in the PDT Window. *Chem. Sci.* **2018**, *9*, 6711–6720.

(18) He, G.; He, M.; Wang, R.; Li, X.; Hu, H.; Wang, H.; Wang, Z.; Lu, Y.; Xu, N.; Du, J.; Fan, J.; Peng, X.; Sun, W. A Near-Infrared Light-Activated Photocage Based on a Ruthenium Complex for Cancer Therapy. *Angew. Chem. Int. Ed.* **2023**, *62*, e202218768.

(19) Liu, Y.; Hammitt, R.; Lutterman, D. A.; Joyce, L. E.; Thummel, R. P.; Turro, C. Ru(II) Complexes of New Tridentate Ligands: Unexpected High Yield of Sensitized $^1O_2$. *Inorg. Chem.* **2009**, *48*, 375–385.

(20) Liu, Y.; Hammitt, R.; Lutterman, D. A.; Thummel, R. P.; Turro, C. Marked Differences in Light-Switch Behavior of Ru(II) Complexes Possessing a Tridentate DNA Intercalating Ligand. *Inorg. Chem.* **2007**, *46*, 6011–6021.

(21) Loftus, L. M.; White, J. K.; Albani, B. A.; Kohler, L.; Kodanko, J. J.; Thummel, R. P.; Dunbar, K. R.; Turro, C. New Ru^{II} Complex for Dual Activity: Photoinduced Ligand Release and $^1O_2$ Production. *Chem. Eur. J.* **2016**, *22*, 3704–3708.

(22) Braddock, J. N.; Meyer, T. J. Kinetics of the Oxidation of $Fe(H_2O)_6^{2+}$ by Polypyridine Complexes of Ruthenium(III). Negative Enthalpies of Activation. *J. Am. Chem. Soc.* **1973**, *95*, 3158–3162.

(23) Loftus, L. M.; Al-Afyouni, K. F.; Rohrabaugh, T. N.; Gallucci, J. C.; Moore, C. E.; Rack, J. J.; Turro, C. Unexpected Role of Ru(II) Orbital and Spin Contribution on Photoinduced Ligand Exchange: New Mechanism to Access the Photodynamic Therapy Window. *J. Phys. Chem. C* **2019**, *123*, 10291–10299.

(24) Warren, J. T.; Chen, W.; Johnston, D. H.; Turro, C. Ground-State Properties and Excited-State Reactivity of 8-Quinolate Complexes of Ruthenium(II). *Inorg. Chem.* **1999**, *38*, 6187–6192.

(25) Rohrabaugh, T. N.; Collins, K. A.; Xue, C.; White, J. K.; Kodanko, J. J.; Turro, C. New Ru(II) Complex for Dual Photochemotherapy: Release of Cathepsin K Inhibitor and $^1O_2$ Production. *Dalt. Trans.* **2018**, *47*, 11851–11858.

(26) Nair, R. B.; Teng, E. S.; Kirkland, S. L.; Murphy, C. J. Synthesis and DNA-Binding Properties of $[Ru(NH_3)_4dppz]^{2+}$. *Inorg. Chem.* **1998**, *37*, 139–141.

(27) Chaires, J. B.; Dattagupta, N.; Crothers, D. M. Studies on Interaction of Anthracycline Antibiotics and Deoxyribonucleic Acid. *Biochemistry* **1982**, *21*, 3933–3940.

(28) Cohen, G.; Eisenberg, H. Viscosity and Sedimentation Study of Sonicated DNA-Proflavine Complexes. *Biopolymers* **1969**, *8*, 45–55.

(29) Evaluation of the p-Bonding Ability of Imidazole: Structure Determination and Characterization of catena-$(H_2O)_2(1\text{-}CH_3im)2Mg(\mu\text{-}CN)(CN)_4(1\text{-}CH_3im)Fe^{III}\bullet H_2O$ (1-CH_3im = 1-Methylimidazole). Johnson, C. R.; Jones, C. M.; Ahser, S. A.; Abola, J. E. *Inorg. Chem.* **1991**, *30*, 210–2129.

(30) Johnson, C. R.; Shepherd, R. E. Mossbauer Study of Imidazole and N-Heterocyclic Complexes of Pentacyanoiron(II) and Pentacyanoiron(III). *Inorg. Chem.* **1983**, *22*, 3506–3513.

(31) Dunbar, M. N.; Steinke, S. J.; Piechota, E. J.; Turro, C. Differences in Photophysical Properties and Photochemistry of Ru(II)-Terpyridine Complexes of CH_3CN and Pyridine. *J. Phys. Chem. A* **2024**, accepted.

(32) Haga, M-A. Synthesis and Protonation-deprotonation Reactions of Ruthenium(II) Complexes Containing 2,2'-Bibenzimidazole and Related Ligands. *Inorg. Chim. Acta* **1983**, *75*, 29-35.

(33) Bernhard, P.; Lehmann, H.; Ludi, A. Synthesis and Properties of Substituted Ruthenium Aqua Complexes. *J. Chem. Soc. Chem. Commun.* **1981**, 1216–1217.

(34) Li, Z. Z.; Niu, Y. L.; Zhou, H. Y.; Chao, H. Y.; Ye, B. H. Visible-Light-Induced Photooxidation of Ruthenium(II) Complex with 2,2'-Biimidazole-like Ligand by Singlet Oxygen. *Inorg. Chem.* **2013**, *52*, 10087–10095.

(35) Zeglis, B. M.; Pierre, V. C.; Barton, J. K. Metallo-Intercalators and Metallo-Insertors. *Chem. Commun.* **2007**, *7345*, 4565–4579.

(36) Kellett, A.; Molphy, Z.; Slator, C.; McKee, V.; Farrell, N. P. Molecular Methods for Assessment of Non-Covalent Metallodrug-DNA Interactions. *Chem. Soc. Rev.* **2019**, *48*, 971–988.

(37) Long, E. C.; Barton, J. K. On Demonstrating DNA Intercalation. *Acc. Chem. Res.* **1990**, *23*, 271–273.

(38) Haq, I.; Lincoln, P.; Suh, D.; Noden, B.; Chowdhry, B. Z.; Chaires, J. B. Interaction of Δ- and Λ-$[Ru(phen)_2DPPX]^{2+}$ with DNA: A Calorimetric and Equilibrium Binding Study. *J. Am. Chem. Soc.* **1995**, *117*, 4788–4796.

(39) Sun, Y.; Lutterman, D. A.; Turro, C. Role of Electronic Structure on DNA Light-Switch Behavior of Ru(II) Intercalators. *Inorg. Chem*. **2008**, *47*, 6427–6434.

(40) Foxon, S. P.; Metcalfe, C.; Adams, H.; Webb, M.; Thomas, J. A. Electrochemical and Photophysical Properties of DNA Metallo-Intercalators Containing the Ruthenium(II) Tris(1-pyrazolyl)methane Unit. *Inorg. Chem.* **2007**, *46*, 409–416.

(41) Foxon, S. P.; Green, C.; Walker, M. G.; Wragg, A.; Adams, H.; Weinstein, J. A.; Parker, S. C.; Meijer, A. J. H. M.; Thomas, J. A. Synthesis, Characterization, and DNA Binding Properties of Ruthenium(II) Complexes Containing Redox Active Ligand Benzo[*i*]dipyrido][3,2-*a:2',3'-c*]phenazine-11,16-quinone. *Inorg. Chem.* **2012**, *51*, 463–471.

(42) Yakovchuk, P.; Protozanova, E.; Frank-Kamenetskii, M. D. Base-Stacking and Base-Pairing Contributions into Thermal Stability of the DNA Double Helix. *Nucleic Acids Res.* **2006**, *34*, 564–574.

(43) Angeles-Boza, A. M.; Bradley, P. M.; Fu, P. K.-L.; Wicke, S. E.; Bacsa, J.; Dunbar, K. R.; Turro, C. DNA Binding and Photocleavage in Vitro by New Dirhodium(II) Dppz Complexes: Correlation to Cytotoxicity and Photocytotoxicity. *Inorg. Chem.* **2004**, *43*, 8510–8519.

(44) Joaqui-Joaqui, M. A.; Maxwell, Z.; Ramakrishnam Raju, M. V.; Jiang, M.; Srivastava, K.; Shao, F.; Arriaga, E. A.; Pierre, V. C. Metallointercalators-DNA Tetrahedron Supramolecular Self-Assemblies with Increased Serum Stability. *ACS Nano* **2022**, *16*, 2928–2941.

(45) Dalton, S. R.; Glazier, S.; Leung, B.; Win, S.; Megatulski, C.; Burgmayer, S. J. N. DNA binding by Ru(II)–bis(bipyridine)–pteridinyl complexes. *J. Biol. Inorg. Chem.* **2008**, *13*, 1133–1148.

(46) Aguirre, J. D.; Lutterman, D. A.; Angeles-Boza, A. M.; Dunbar, K. R.; Turro, C. Effect of Axial Coordination on the Electronic Structure and Biological Activity of Dirhodium(II,II) Complexes. *Inorg. Chem.* **2007**, *46*, 7494–7502.

(47) Chen, X.; Gao, F.; Yang, W.-Y.; Zhou, Z.-X.; Lin, J.-Q.; Ji, L.-N. Structure-Activity Relationship of Polypyridyl Ruthenium(II) Complexes as DNA Intercalators, DNA Photocleavage Agents, and DNA Topoisomerase and RNA Polymerase Inhibitors. *Chem. Biodiver.* **2013**, *10*, 367–384.

(48) Frodl, A.; Herebian, D.; Sheldrick, W. S. Coligand Tuning of the DNA Binding Properties of Bioorgano-metallic (η^6-Arene)Ru(II) Complexes of the Type (η^6-Arene)Ru(amino acid)(dppz)]$^{n+}$ (dppz = dipyrido[3,2-*a:2'3'-c*]phenazine), n = 1 – 3. *J. Chem. Soc. Dalton Trans.* **2002**, 3664–3673.

(49) Suh, D.; Chaires, J. B. Criteria for the Mode of Binding of DNA Binding Agents. *Bioorganic Med. Chem.* **1995**, *3*, 723–728.

(50) Aguirre, J. D.; Angeles-Boza, A. M.; Chouai, A.; Pellois, J.-P.; Turro, C.; Dunbar, K. R. Live Cell Cytotoxicity Studies: Documentation of the Interactions of Antitumor Active Dirhodium Compounds with Nuclear DNA. *J. Am. Chem. Soc.* **2009**, *131*, 11353–11360.

(51) Lutterman, D. A.; Chouai, A.; Liu, Y.; Sun, Y.; Stewart, C. D.; Dunbar, K. R.; Turro, C. Intercalation is Not Required for DNA Light-Switch Behavior. *J. Am. Chem. Soc.* **2008**, *130*, 1163–1170.

(52) Aguirre, J. D.; Angeles-Boza, A. M.; Chouai, A.; Turro, C.; Pellois, J.-P.; Dunbar, K. R. Anticancer Activity of Heteroleptic Diimine Complexes of Dirhodium: A Study of Intercalating Properties, Hydrophobicity, and In Cellulo Activity. *Dalton Trans*. **2009**, 10806–10812.

(53) Gray, D. M. Circular Dichroism of Protein-Nucleic Acid Interactions. In *Circular Dichroism and the Conformational Analysis of Biomolecules*; Fasman, G. D., Ed.; Spring Science+Business Media: New York, 1996; pp 469–500.

(54) Schäfer, S.; Ott, I.; Gust, R.; Sheldrick, W. S. Influence of the Polypyridyl (pp) Ligand Size on the DNA Binding Properties, Cytotoxicity and Cellular Uptake of Organoruthenium(II) Complexes of the Type [(η^6-C_6Me_6)Ru(L)(pp)]$^{N+}$ [L = Cl, n = 1; L = (NH_2CS, n = 2. *Eur. J. Inorg. Chem.* **2007**, 3034–3046.

(55) Dalgleish, D. G.; Peacocke, A. R.; Fey, G.; Harvey, C. The Circular Dichroism in the Ultraviolet of Aminoacridines and Ethidium Bromide Bound to DNA. *Biopolymers* **1971**, *10*, 1853–1863.

(56) Huang, C. H.; Baserga, R. Circular Dichroism Studies of Ethidium Bromide Binding to the Isolated Nucleolus. *Nucleic Acids Res.* **1976**, *3*, 1857–1873.

(57) Gençaslan, S.; Sheldrick, W. S. Bifunctional Bioorganometallic Iridium(III)-Platinum(II) Complexes Incorporating Both Intercalative and Covalent DNA Binding Capabilities. *Eur. J. Inorg. Chem.* **2005**, 3840–3849.

(58) Kelly, J. M.; Tossi, A. B.; McConnell, D. J.; OhUigin, C. A Study on the Interactions of Some Polypyridylruthenium(II) Complexes with DNA Using Fluorescence Spectroscopy, Topoisomerisation and Thermal Denaturation. *Nucleic Acids Res.* **1985**, *13*, 6017–6034.

(59) Liu, Y.; Hammitt, R.; Lutterman, D. A.; Joyce, L. E.; Thummel, R. P.; Turro, C. Ru(II) Complexes of New Tridentate Ligands: Unexpected High Yield of Sensitized $^1O_2$. *Inorg. Chem.* **2009**, *48*, 375–385.

(60) Sun, Y.; Joyce, L. E.; Dickson, N. M.; Turro, C. DNA Photocleavage by an Osmium(II) Complex in the PDT Window. *Chem. Commun.* **2010**, *46*, 6759–6761.

TOC Graphic

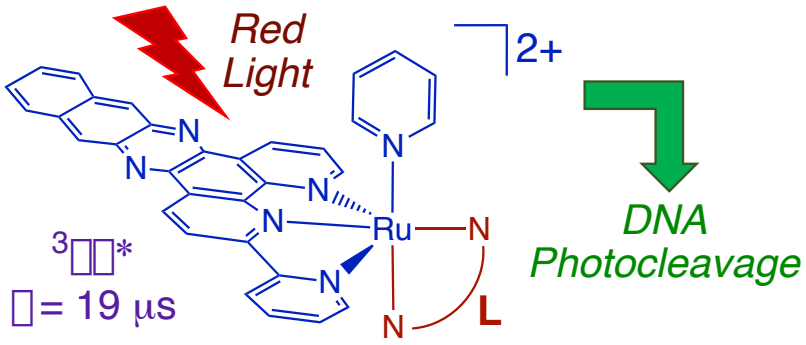

Synopsis

Two complexes containing the tridentate ligand pydppn, pyridine, and a bindentate ligand, bpy (2,2'-bipyridine; **1**), bim (2,2'-bisimidazole; **2**), Me4bim (2,2'-bis(4,5-dimethylimidazole; **3**), possess long-lived pydppn-centered excited states accessible with red light. Thermal denaturation, circular dichroism, and electronic absorption experiments show that the complexes intercalate between the DNA bases. The absorption of **2** and **3** tail into the PDT window, produce $^1O_2$, and **3** is able to photocleave plasmid DNA upon 655 nm irradiation.